Beam Physics Note
TRI-BN-24-06
March 6, 2024

Comparison of Envelope Tracking at cERL Injection

H. W. Koay

TRIUMF

Abstract: This report discusses the comparison of envelope tracking between different envelope tracking code: TRANSOPTR and GPT. The beam size is further compared with real beam data obtained at cERL. Overall the results from TRANSOPTR agree rather well with GPT and the real data.

1 Introduction

In order to investigate the space charge effect (SC) in the lower energy section, the envelope tracking from two different simulations were compared using the injector section in the cERL beam line. One of simulations is a multi-particle tracking code named General Particle Tracking (GPT), whereas the other one is a second-order beam transport code TRANSOPTR.

2 Layout of cERL

Tracking in GPT starts from the GUN up to before the the first bender BMAG01. The injector layout at cERL is shown in Fig. 1.

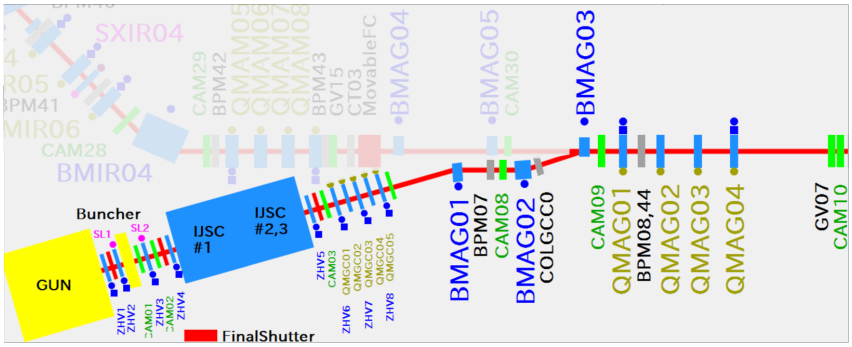

Figure 1: The layout of the beamline for the cERL injector.

3 Comparison between simulations

3.1 Field map and parameters

The overlay of EM field from the gun, solenoids and RF along the beamline is given in Fig. 2. Note that both RF cavity and solenoid field has axial symmetry effect in TRANSOPTR. Therefore, only the on-axis 1D field is used in TRANSOPTR.

3.2 Initial distribution

The initial distribution used in GPT assumed a Gaussian distribution with no correlation among x, y and z:

$$\begin{aligned} \textbf{transverse}: \ & \sigma_x = 0.84\,\text{mm}, \text{ with } 3\sigma \text{ cutoff} \\ \textbf{longitudinal}: \ & \sigma_z = 3\text{ps}, \text{ with } 3\sigma \text{ cutoff} \end{aligned} \tag{1}$$

In TRANSOPTR, two tracking were performed using starting from (A) s=0 cm, (B)

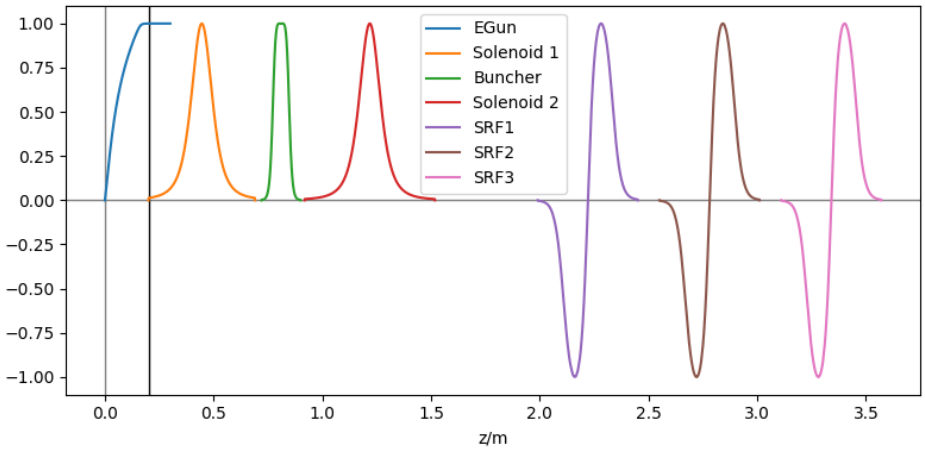

Figure 2: The E/M field of the cERL injection beamline. The orange and red curves are the magnetic field of the first and second solenoid, while the blue curve is the axial potential across the egun. The green curve is the buncher axial potential, while the purple, brown and pink curves are the one for the injector cavity 1, 2 and 3 respectively. Note that all the voltages and magnetic fields are normalized, so that they are unitless. The black vertical line at z=0.2 m indicates the starting point of TRANSOPTR simulation. It has the least effect from the surrounding E/M field.

s=20 cm. The main difference between (A) and (B) is the inclusion of electron gun (e-gun) to accelerate beam produced from the cathode at energy < 1 eV to 450 keV, whereas for (B), tracking starts right after the e-gun.

(A) Starting point at s=0 cm As for tracking starting from s=0 cm, the average beam energy starts at 0.18 eV The initial condition as follow was used (note that the sigma here indicates the full envelope in sigma matrix instead of standard deviation in 1):

$$\begin{aligned} \sigma_{11} = \sigma_{33} &= \sqrt{5}\sigma_x = 0.259\,\text{cm} \\ \sigma_{22} = \sigma_{44} &= 1.0 \\ \sigma_{55} &= \sqrt{5}\sigma_z = 0.000167\,\text{cm} \\ \sigma_{66} &= \sqrt{5}\sigma_{p_z} = 0.0027 \\ \text{r12= r34=r56} &= 0.0 \end{aligned}$$

An example of the transverse velocity distribution at s=0 cm is shown in Fig. 3b. The velocity is uniformly distributed in x,y and z from the cathode in the GPT simulation. This explains why the maximum transverse angle $\sigma_{22} = \sigma_{44} = 1.0$ ($\sigma_{22} = \frac{p_x}{p_0}$, $\sigma_{44} = \frac{p_y}{p_0}$). Note that the maximum $\sigma_{22} = 1.0$ as $p_x \leq p_0$.

(B) Starting point at s=20 cm On the other hand, tracking starting from s=20 cm uses different Twiss parameters fitted from the GPT calculations at s=20 cm at different bunch

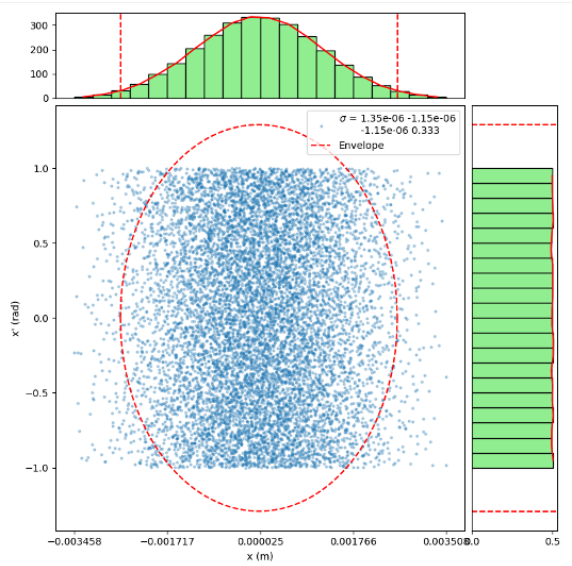

(a) The transverse phase space distribution (x, x') .

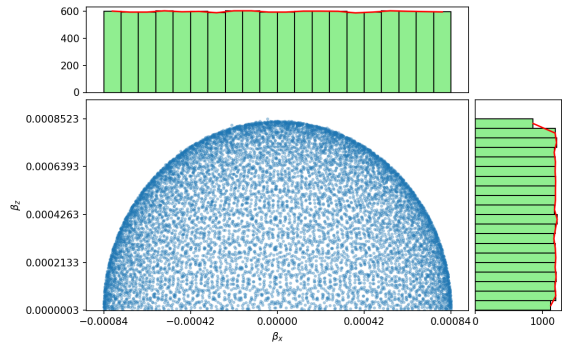

(b) The normalized velocity distribution.

Figure 3: The initial distribution used in GPT at s=0 cm.

charges. The phase space distributions are shown in Fig. 4.

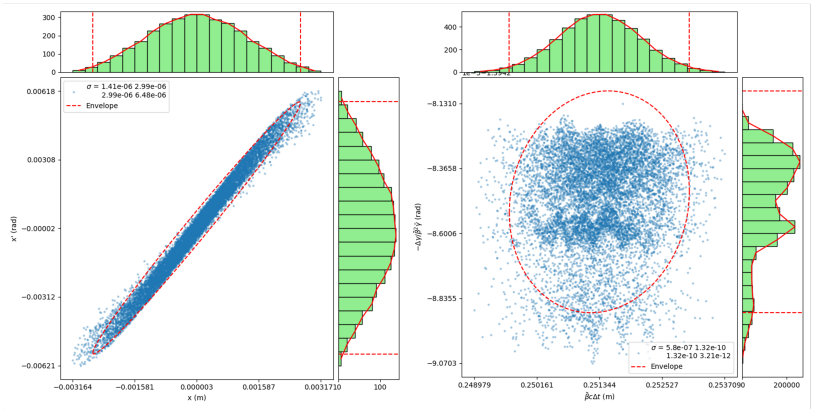

(a) No space charge

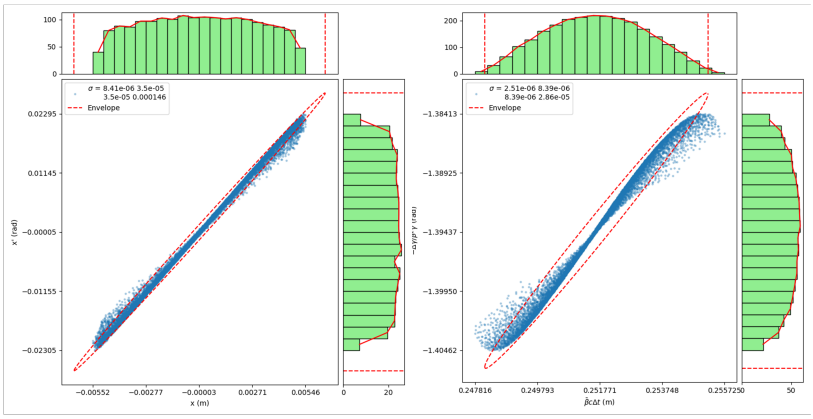

(b) 60 pC

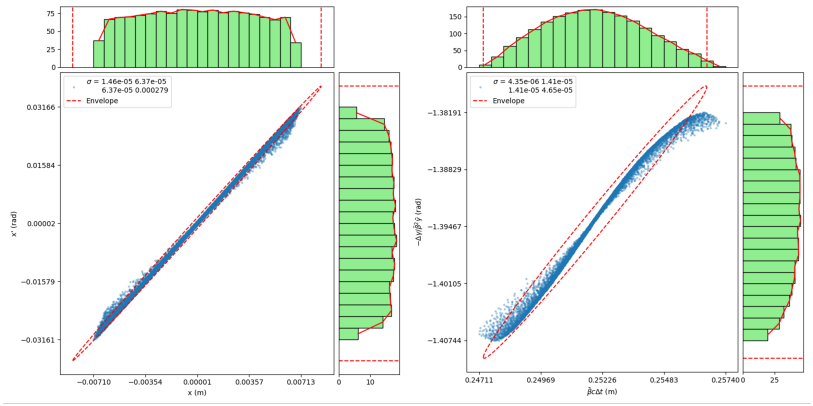

(c) 110 pC

Figure 4: The phase space beam distribution at z=20 cm at different bunch charges. *Left:* Transverse plot of x VS $\frac{p_x}{P_0}$ or y VS $\frac{p_y}{P_0}$ (assuming round beam). *Right:* Longitudinal plot of $z = \Delta t \beta c$ VS $-\frac{\Delta\gamma}{\gamma\beta^2}$

3.3 Results

(A) Starting point at s=0 cm The comparison of results are shown in Fig. 5. Three different bunch charges were compared: no SC, 60 pC and 110 pC. The injector phases were fine tuned for max energy gain. The final beam energy after passing through the injector is about 3 MeV.

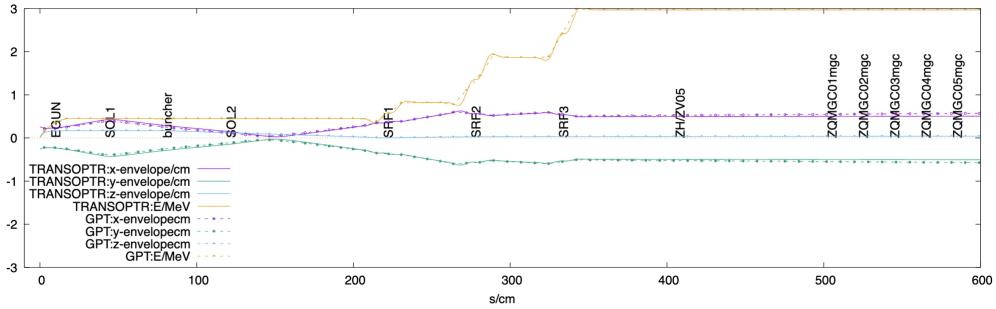

(a) No space charge

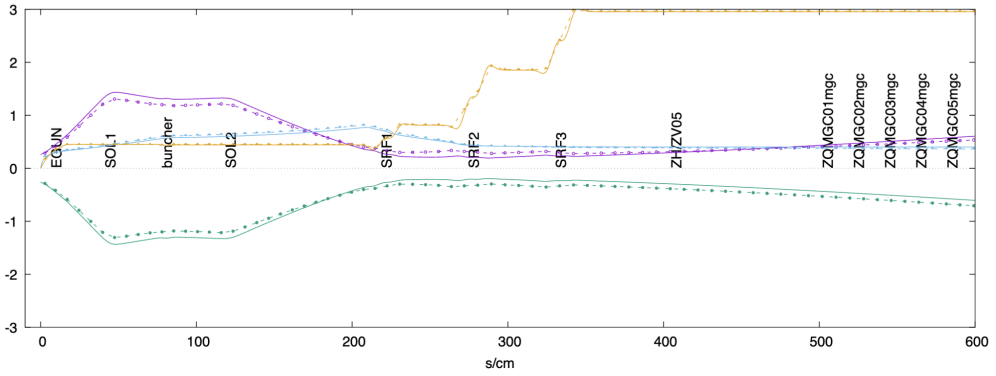

(b) 60 pC

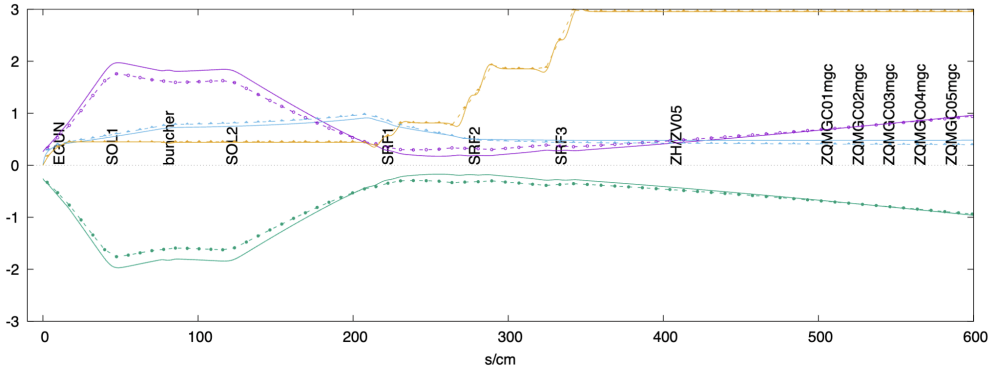

(c) 110 pC

Figure 5: (A) The comparison of transverse beam envelope between TRANSOPTR (solid) and GPT (dashed) at different bunch charges. This corresponds to TRANSOPTR simulation starting from s=0 cm. The initial condition for three different space charges is the same.

(B) Starting point at s=20 cm The comparison of results are shown in Fig. 5 and (B) Fig. 6 (from s=20 cm).

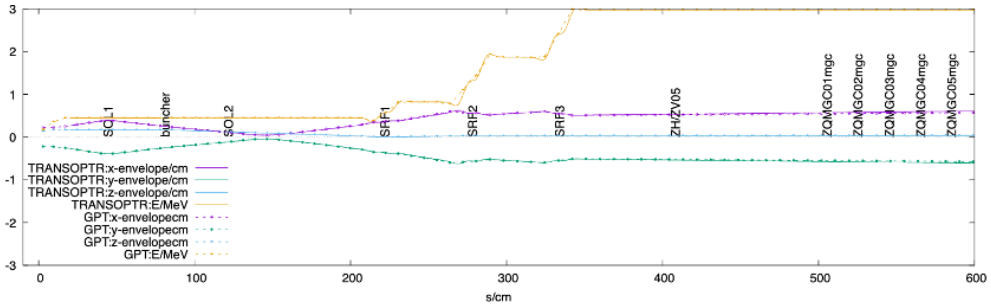

(a) No space charge

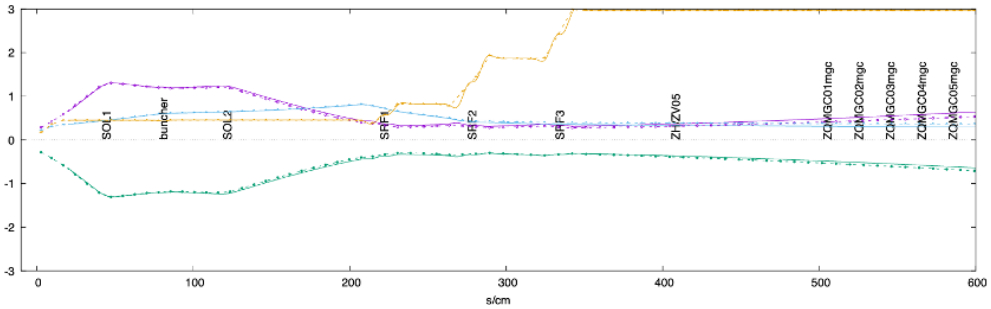

(b) 60 pC

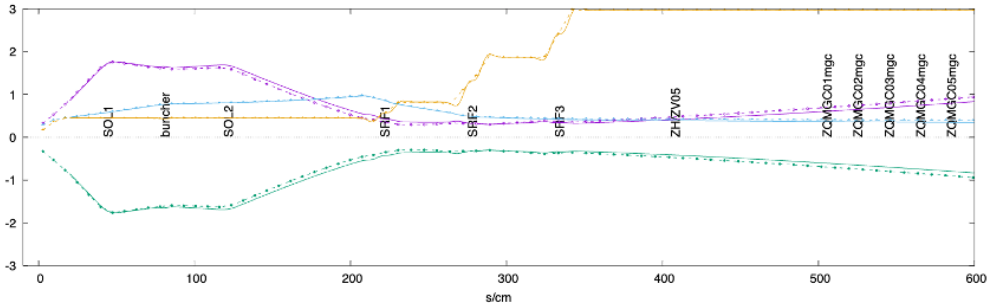

(c) 110 pC

Figure 6: (B) The comparison of transverse beam envelope between TRANSOPTR (solid) and GPT (dashed) at different bunch charges. The TRANSOPTR simulation starting from s=20 cm

Generally, the match of (B) is better than (A): the match between these two codes is within ±10% when (A) and ±2%. This is the case even for no SC. This could be due to the assumption of $\frac{P_x}{P} << 1$ is not valid at the early stage of beam production ($\frac{P_x}{P} = 1$ for this case). Therefore, Hamiltonian up to only second order seems insufficient. More information can refer to Appendix B. Overall, the match is the best for no SC in both (A) and (B). However, the discrepancy for 110 pC is slightly larger for (A).

4 Comparison of TRANSOPTR with real beam

4.1 Calibration of laser intensity and bunch charge

First, calibration of laser intensity at different bunch charges was performed using the Faraday's cup located at the gun. The calibration results is shown as follows:

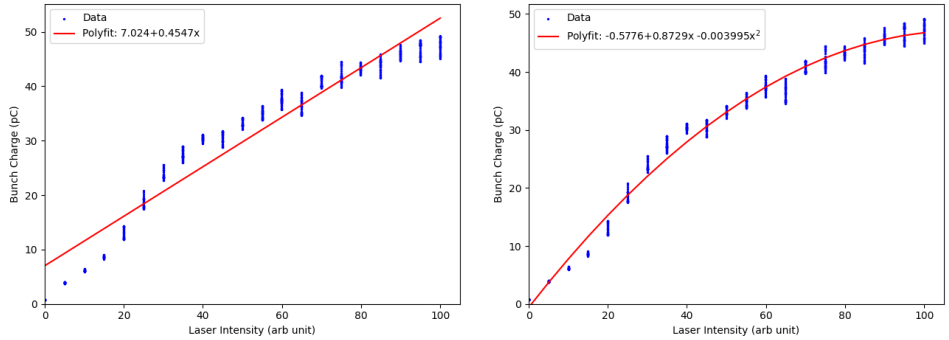

(a) Linear fit (b) Quadruatic fit

Figure 7: The first and second order fit of the laser intensity to bunch charge. The second order curve fits better. Hence, it is used in the following work to estimate the bunch charge.

4.2 Comparison of beam size

Sigma of the Gaussian fitted beam is measured at CAM01 using different solenoid currents. An example of the beam image is shown in Fig. 8.

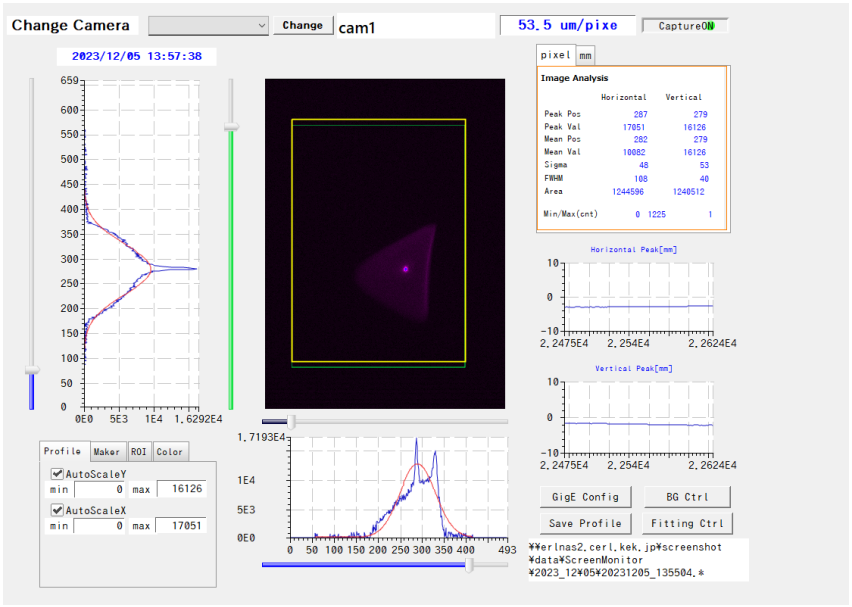

Figure 8: The beam seen on CAM01 using real beam at 50 pC.

The data taken is then fitted with the TRANSOPTR calculations to determine the best initial condition (IC) at s=0 cm for all bunch charges. A round beam ($x = y$) is assumed here. The results of solenoid scans are shown in Fig, 9.

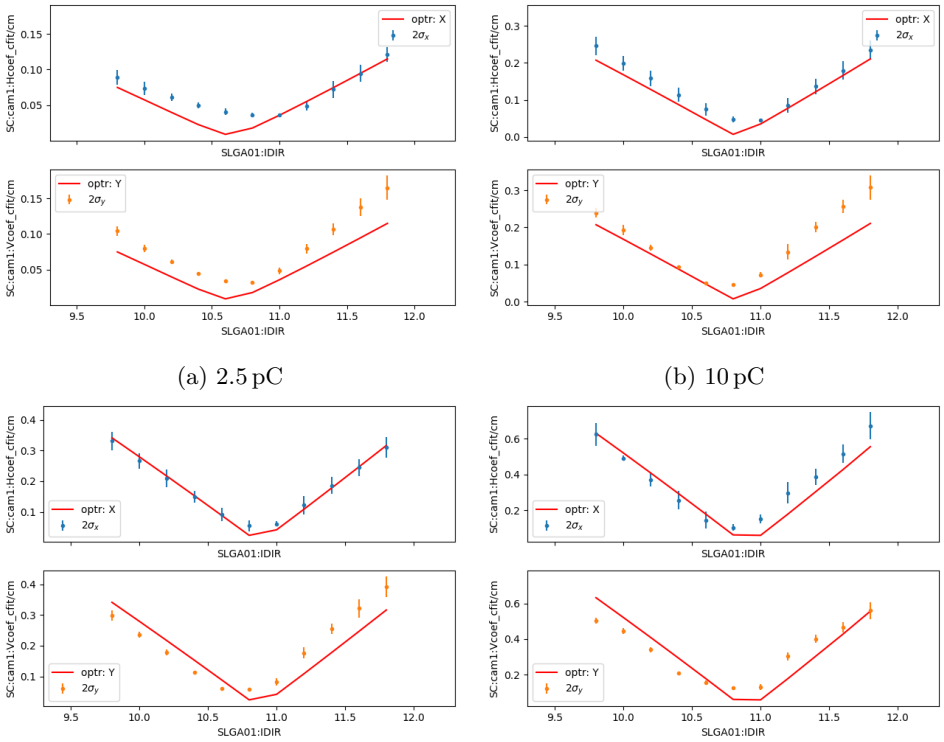

(a) 2.5 pC (b) 10 pC

(c) 20 pC (d) 50 pC

Figure 9: Solenoid scan comparing real beam and TRANSOPTR at CAM01 to find the best-fitted initial conditions for all bunch charges. The best fitted IC in TRANSOPTR are given as $(x, x', z, z') = (0.0654, 1.0, 0.00225, 0.0004666)$ at initial energy of 0.187 eV (the same as the in the comparison with GPT).

The best-fitted IC were then used to track the beam until CAM02 (as shown in Fig 10). The experimental beam size at CAM02 is then compared with the tracked values from TRANSOPTR. The results are shown in Fig. 11.

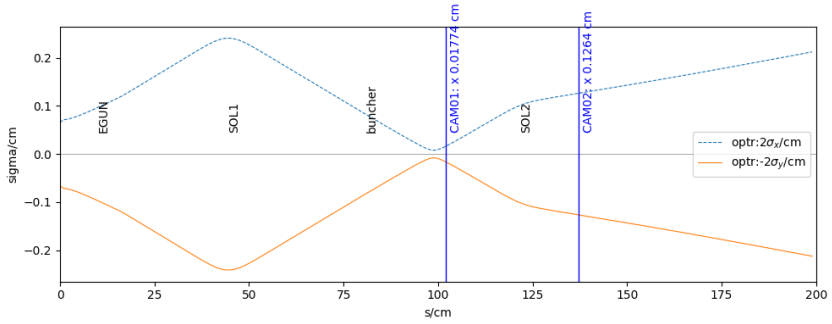

Figure 10: An example showing the envelope fitted with the IC from Fig. 9. The beam size obtained at CAM02 is then compared again with the experimental data.

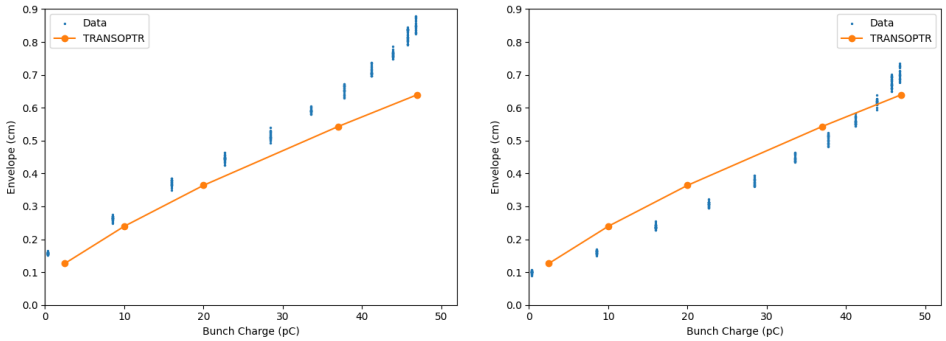

(a) X (b) Y

Figure 11: Comparison of beam size between TRANSOPTR and real beam at CAM02 using the best-fitted IC from Fig. 9. Note that the experimental beam size is just a Gaussian-fitted sigma; it is NOT the rms of the beam.

Appendix A Max. sixth coordinate in TRANSOPTR

The sixth coordinate, σ_{66}, in TRANSOPTR is given as:

$$\sigma_{66} = \frac{\Delta E}{\beta c}\frac{1}{p_0} \tag{2}$$

If T, the kinetic energy, is the maximum ΔE ($\Delta E_{\max} = T$) at $\gamma \approx 1$ (for instance right after the cathode),

$$\Delta E_{\max} = T = \frac{mv^2}{2}$$
$$p_0 = mv\sigma_{66} = \frac{mv^2}{2}\frac{1}{mv \cdot v} = \frac{1}{2}$$

Therefore, when energy is small and $\gamma \approx 1$, the maximum $\sigma_{66} = 0.5$.

Appendix B F-matrix of Egun

This section mainly discussed the work from [1], but in a more detailed way for better understanding. Space charge is omitted here to simplify the formalism. This F-matrix is similar to the algorithm used in TRANSOPTR, but including SC.

Appendix B.1 Series representation of axisymmetric electric field

Laplace equation of an axisymmetric field potential $V(r, z)$ is given as follows:

$$\nabla^2 V(r,z) = \frac{1}{r}\frac{\partial}{\partial r}\left(r\frac{\partial V}{\partial r}\right) + \frac{\partial^2 V}{\partial z^2} = 0 \tag{3}$$
$$V(r,z) = V_0(z) + V_1(z)r + V_2(z)r^2 + ...$$

where $V_0(z) = V(r = 0, z)$ is the on-axis potential. Due to axisymmetric nature, $\frac{\mathrm{d}V}{\mathrm{d}r}(r = 0, z) = E_r(r = 0, z) = 0$. Thus,

$$V(r,z) = V_0(z) + V_2(z)r^2 + V_4(z)r^4 + ... \tag{4}$$
$$= \sum_{i=0}^{\infty} V_{2i}(z)r^{2i}$$

Differentiating eq. 4 acording to 3,

$$\nabla^2 V(r,z) = 4V_2 + 16V_4 r^2 + V_0''(z) + V_2''(z)r^2 + \mathcal{O}(r^4) = 0$$

When $r = 0$,

$$\begin{aligned} 4V_2 + V_0''(z) &= 0 \\ V_2 &= -\frac{1}{4}V_0''(z) \end{aligned} \tag{5}$$

Substituting 5 into 4,

$$V(r,z) = V_0(z) - \frac{1}{4}V_0''(z)r^2 + \mathcal{O}(r^4)... \tag{6}$$

Appendix B.2 Hamiltonian for axially symmetry electric field

The Hamiltonian H, with the independent variable s, when passing through a DC accelerator column (such as the e-gun) that has zero magnetic field is given by:

$$H(x, P_x, y, P_y, t, E; s) = -\sqrt{\left(\frac{E - qV(x,y,s)}{c}\right)^2 - m^2c^2 - P_x^2 - P_y^2} \tag{7}$$

where P_x and P_y are the canonical momentum conjugate to the transverse x and y, m is the mass, and V is the potential energy as given in eq. 6.

Taking $P^2 = \frac{E - qV_0(s))^2}{c^2} - m^2c^2 = \beta\gamma mc$:

$$\begin{aligned} \left(\frac{E - qV(x,y,s)}{c}\right)^2 &= \left(\frac{E - qV_0}{c}\right)^2 + \frac{(x^2+y^2)qV_0''}{2c^2}\left(E - qV_0 - qV_0''\frac{x^2+y^2}{8}\right) \\ &= \left(P^2 + m^2c^2\right) + \frac{(x^2+y^2)qV_0''}{2c^2}\left(\gamma mc^2 + \mathcal{O}(q^4)...\right) \end{aligned} \tag{8}$$

As only the second order terms are included, drop $\mathcal{O}(q^4)$ and substitute eq. 8 into 7

$$\begin{aligned} H(x, P_x, y, P_y, t, E; s) &= -\sqrt{P^2 + \frac{(x^2+y^2)qV_0''}{2c^2}(\gamma mc^2) - P_x^2 - P_y^2} \\ &= -P\sqrt{1 + \frac{(x^2+y^2)qV_0''}{2Pc^2}\frac{\gamma mc^2}{\beta\gamma mc} - \frac{P_x^2}{P^2} - \frac{P_y^2}{P^2}} \\ &= -P\sqrt{1 + \frac{(x^2+y^2)qV_0''}{2P\beta c} - \frac{P_x^2}{P^2} - \frac{P_y^2}{P^2}} \end{aligned} \tag{9}$$

Expanding 9 up to $\mathcal{O}(q^2)$, where q is x, y, P_x, P_y,

$$\begin{aligned} H(x, P_x, y, P_y, t, E; s) &\approx -P\left[1 + \frac{(x^2+y^2)qV_0''}{4P\beta c} - \frac{P_x^2}{2P^2} - \frac{P_y^2}{2P^2}\right] \\ &\approx -P - \frac{(x^2+y^2)qV_0''}{4\beta c} + \frac{P_x^2}{2P} + \frac{P_y^2}{2P} \end{aligned} \tag{10}$$

Expanding $P = \sqrt{\frac{(E-qV)^2}{c^2} - m^2c^2}$ using $E = E_0 + \Delta E$,

$$\begin{aligned} P &= \sqrt{\frac{(E_0 + \Delta E - qV)^2}{c^2} - m^2c^2} \\ &= \sqrt{\frac{(E_0 - qV)^2}{c^2} - m^2c^2 + \frac{\Delta E^2}{c^2} + \frac{2\Delta E\gamma_0 mc^2}{c^2}} \end{aligned}$$

Taking $P_0 = \sqrt{\frac{(E_0-qV)^2}{c^2} - m^2c^2} = \beta_0\gamma_0 mc$, expanding P up to second order of ΔE,

$$\begin{aligned} P &= P_0\sqrt{1 + \frac{\Delta E^2}{P_0^2c^2} + \frac{2\Delta E\gamma_0 m}{P_0^2}} \\ &\approx P_0\left[1 + \frac{\Delta E^2}{2P_0^2c^2} + \frac{2\Delta E\gamma_0 m}{2P_0^2} - \frac{1}{8}\left(\frac{2\Delta E\gamma_0 m}{P_0^2}\right)^2\right] \\ &\approx P_0 + \frac{\Delta E^2}{2P_0c^2} + \frac{\Delta E\gamma_0 m}{\beta_0\gamma_0 mc} - \frac{1}{2}\frac{\Delta E^2\gamma_0^2 m^2}{P_0^3} \\ &\approx P_0 + \frac{\Delta E}{\beta_0 c} + \frac{\Delta E^2}{2P_0c^2}\left[1 - \frac{1}{\beta_0^2}\right] \\ &\approx P_0 + \frac{\Delta E}{\beta_0 c} + \frac{\Delta E^2}{2P_0c^2}\left[-\frac{1}{\gamma_0^2\beta_0^2}\right] \\ &\approx P_0 + \frac{\Delta E}{\beta_0 c} - \frac{\Delta E^2}{2\gamma_0^3\beta_0^3 mc^3} \end{aligned}$$

Substitute this into eq. 10,

$$H(x, P_x, y, P_y, t, E; s) = -P_0 - \frac{\Delta E}{\beta_0 c} + \frac{\Delta E^2}{2\gamma_0^3\beta_0^3 mc^3} - \frac{(x^2+y^2)qV_0''}{4\beta c} + \frac{P_x^2 + P_y^2}{2P} \tag{11}$$

Appendix B.3 Generating function to change variables

Changing the canonical conjugate from $(t, -E)$ to (z, P_z) can be done in two stages. First, it is changed from $(t, -E)$ to $(\Delta t, -\Delta E)$, then to (z, P_z).

Appendix B.3.1 Changing from $(t, -E)$ to $(\Delta t, -\Delta E)$

The generating function of the second type, $G(\mathbf{P}; q; s)$ can used:

$$\begin{aligned} G &= -\left(t - \int \frac{ds}{\beta_0 c}\right)(\Delta E + E_0) \\ \frac{\partial G}{\partial s} &= \frac{E_0 + \Delta E}{\beta_0 c} \\ \frac{\partial G}{\partial t} &= -E \\ \frac{\partial G}{\partial(-\Delta E)} &= \Delta t \end{aligned}$$

The new Hamiltonian $H_{\Delta t} = H_t + \frac{\partial G}{\partial s}$ is now

$$H(x, P_x, y, P_y, \Delta t, -\Delta E; s) = \frac{E_0}{\beta_0 c} - P_0 + \frac{\Delta E^2}{2\gamma_0^3 \beta_0^3 mc^3} - \frac{(x^2+y^2)qV_0''}{4\beta c} + \frac{P_x^2 + P_y^2}{2P} \quad (12)$$

Appendix B.3.2 Changing from $(\Delta t, -\Delta E)$ to (z, P_z)

Similarly, generating function of the second type $G(\mathbf{P}; q; s)$ is used (taking $(z, P_z) = (-\beta_0 c\Delta t, \Delta E/\beta_0 c)$

$$\begin{aligned} G &= -\beta c \Delta t P_z \\ \frac{\partial G}{\partial s} &= \frac{\beta'}{\beta} z P_z \\ \frac{\partial G}{\partial \Delta t} &= -\Delta E \\ \frac{\partial G}{\partial P z} &= -\beta c \Delta t = z \end{aligned}$$

The new Hamiltonian $H_z = H_{\Delta t} + \frac{\partial G}{\partial s}$ is now

$$\begin{aligned} H(x, P_x, y, P_y, z, P_z; s) = \frac{\beta'}{\beta} z P_z + \frac{E_0}{\beta_0 c} - P_0 + \frac{P_z^2 \beta^2 c^2}{2\gamma_0^3 \beta_0^3 mc^3} \\ - \frac{(x^2+y^2)qV_0''}{4\beta c} + \frac{P_x^2 + P_y^2}{2P} \end{aligned} \quad (13)$$

Assuming $\beta \approx \beta_0$ for $\Delta E << E_0$,

$$H(x, P_x, y, P_y, z, P_z; s) = \frac{\beta'}{\beta} z P_z + \frac{E_0}{\beta_0 c} - P_0 + \frac{P_z^2}{2\gamma_0^2 P_0} - \frac{(x^2+y^2)qV_0''}{4\beta c} + \frac{P_x^2 + P_y^2}{2P} \quad (14)$$

Appendix B.4 Hessian matrix of hamiltonian

The first order derivative of Hamiltonian from eq. 14 is zero when $(x, P_x, y, P_y, z, P_z) = (0, 0, 0, 0, 0, 0)$.

The second order derivative of Hamiltonian (also known as the Hessian Matrix, $\mathcal{H}$),

$$\mathcal{H} = \begin{pmatrix} \frac{\partial^2 H}{\partial x_1^2} & \frac{\partial^2 H}{\partial x_1 \partial x_2} & \cdots & \frac{\partial^2 H}{\partial x_1 \partial x_6} \\ \frac{\partial^2 H}{\partial x_2 \partial x_1} & \frac{\partial^2 H}{\partial x_2^2} & \cdots & \frac{\partial^2 H}{\partial x_2 \partial x_6} \\ \vdots & \vdots & \ddots & \vdots \\ \frac{\partial^2 H}{\partial x_6 \partial x_1} & \frac{\partial^2 H}{\partial x_6 \partial x_2} & \cdots & \frac{\partial^2 H}{\partial x_6^2} \end{pmatrix}$$

with $(x_1, x_2, x_3, x_4, x_5, x_6) = (x, P_x, y, P_y, z, P_z)$

Appendix B.5 Infinitesimal matrix of DC accelerating column

The infinitesimal transfer matrix $F(s)$ is defined as

$$\frac{\mathrm{d}\mathbf{x}}{\mathrm{d}s} = F\mathbf{x}$$

$$\mathbf{x} = \begin{pmatrix} x \\ p_x \\ y \\ p_y \\ z \\ p_z \end{pmatrix}$$

Note that all p_x, p_y and p_z are the normalized momenta in TRANSOPTR, i.e. $p_x = \dfrac{P_x}{P}$ and so. The corresponding F matrix can be obtained by taking the product between the Hessian Matrix $\mathcal{H}$) and S

$$S = \begin{pmatrix} 0 & 1 & 0 & 0 & 0 & 0 \\ -1 & 0 & 0 & 0 & 0 & 0 \\ 0 & 0 & 0 & 1 & 0 & 0 \\ 0 & 0 & -1 & 0 & 0 & 0 \\ 0 & 0 & 0 & 0 & 0 & 1 \\ 0 & 0 & 0 & 0 & -1 & 0 \end{pmatrix} \tag{15}$$

$$F = \begin{pmatrix} 0 & \dfrac{1}{P} & 0 & 0 & 0 & 0 \\ \frac{qV_0''}{2\beta c} & 0 & 0 & 0 & 0 & 0 \\ 0 & 0 & 0 & \dfrac{1}{P} & 0 & 0 \\ 0 & 0 & \frac{qV_0''}{2\beta c} & 0 & 0 & 0 \\ 0 & 0 & 0 & 0 & \dfrac{\beta'}{\beta} & \frac{1}{P\gamma^2} \\ 0 & 0 & 0 & 0 & 0 & -\dfrac{\beta'}{\beta} \end{pmatrix} \tag{16}$$

The F-matrix including SC is not discussed here as this is just to provide an insight for the derivation of the DC accelerating column. More work integrating SC can be found in [1].

References

[1] R. A. Baartman, Bunch Dynamics through Accelerator Column, Conf. Proc. C 110904 (2011) 649–651.